MECHANICAL CHARACTERISATION AND MODELLING OF A THERMOREVERSIBLE SUPERAMOLECULAR POLYURETHANE OVER A WIDE RANGE OF RATES

Huanming. Chen[1*], Lewis. R. Hart[2], Wayne. Hayes[2], Clive.R. Siviour[1]

[1]Solid Mechanics and Materials Engineering Department of Engineering Science

University of Oxford, Oxford, United Kingdom, OX1 3PJ

[2]Department of Chemistry

University of Reading, Reading, United Kingdom, RG6 6DX

∗huanming.chen@eng.ox.ac.uk

ABSTRACT

Understanding the mechanical response of thermo-recoverable elastomers to applied deformation at different strain rates and temperatures is crucial for more effective exploitation of these reusable materials in industrial applications. The research presented in this paper aims to understand the thermal and mechanical responses of a healable, elastomeric supramolecular polyurethane, examining morphology, rheology and mechanical responses from low to high strain rates. In particular, measurement of the high strain rate response of low modulus, or low strength, materials is challenging, and the current paper addresses this by incorporating a modelling framework based on low-rate characterization. To support this research, significant characterization experiments have been performed, which also show, for the first time, the excellent reusability of the polymer. The structure of specimens with different thermal histories was characterized using nuclear magnetic resonance spectroscopy, gel permeation chromatography and small angle X-ray scattering. Differential scanning calorimetry and Rheometry were used to investigate thermomechanical performance during heating and cooling cycles, whilst large strain compression characterization was performed on a commercial screw-driven test frame, a hydraulic loading system and a split-Hopkinson pressure bar. To describe the mechanical response of the polymer, a viscoelastic softening

model was developed and characterized. The model incorporates data from rheometry and dynamic mechanical analysis using the principle of time-temperature superposition in a Prony series, combined with a non-linear large strain response, and recovery. The model was able to describe low strain rate behaviour under monotonic and cyclic loading, as well as predicting the response to monotonic loading at medium-to-high strain rates from 40 to 1220 s^{-1}. The paper therefore demonstrates the effectiveness of using the viscoelastic theory and its analytical model to calibrate and further predict the mechanical behaviour of polymers at different strain rates: this is particularly useful for low modulus materials for which high strain rate characterization is challenging.

Keywords: Viscoelasticity, Polyurethane, Healability, DMA, Morphology, High strain-rate

Highlights:

- Characterization and modelling of a supramolecular polyurethane with healing capability.
- Structural and mechanical properties measured using wide range of techniques
- Data show consistent response over multiple thermal cycles: reusability and recyclability.
- Model predicts high-rate response from static data, avoiding high strain rate characterization.

1 Introduction

The development of healable polymers that are capable of repairing damage either on the surface or within the bulk material is an extremely attractive proposition in many industrial applications, with potential to significantly reduce whole life costs and environmental impact [1]. Whilst a number of methodologies to achieve healable materials are known [2], supramolecular materials offer an attractive solution owing to their inherent ability to undergo multiple break/heal cycles without significant loss of performance [3][4]. Recent research has led to the development of specifically designed healable supramolecular polyurethanes (SPU) [5–10] which exhibit thermally-controlled mechanics and recoverable mechanical properties resulting from the use of dynamic and reversible non-covalent interactions such as hydrogen bonds and π-π stacking interactions in the polymer network [1,7,8,11–15]. In previous research, the synthesis of a polyurethane with excellent healing ability at around body temperature has been reported [8], where, following damage, the material's mechanical properties could be recovered efficiently by re-assembly of the supramolecular network. Specifically, the polymer possesses complementary hydrogen bonding motifs which are able to self-assemble, in addition to secondary self-assembly though π-π stacking of the aryl units within the diisocyanate [16][17]. Furthermore, micro phase separation is observed between the apolar polymer backbone and the polar recognition motifs. It has been demonstrated that purification of the SPU is not necessary as the low molecular weight bis-urea by product is able to reinforce the polymer network and impart desirable mechanical properties [18–20]. The nature of these non-covalent interactions permits the material, in common with other supramolecular polyurethanes [21–23], to be addressable as a result of its inherent thermo-responsive character of the supramolecular interactions, thereby delivering dramatic viscosity changes over well-defined and tuneable temperature ranges, as well as leading to the capability to recover a significant degree of their mechanical strength after damage. As a result of the non-covalent interactions within the network being relatively weak, the recognition motifs within the polymer can

assemble or dissociate relatively easily as a consequence of the low thermal activation energy, making it, in common with other supramolecular polyurethanes and polyureas, easy to process at relatively low temperatures [24–26].

In previous research, the material properties of the supramolecular polyurethane have been characterized using dynamic mechanical analysis (DMA) and tensile tests, which revealed a mechanical response that is very sensitive to temperature [8]. However, further understanding of the large-strain mechanical properties is needed for application of the material. In order to use these materials in engineering applications such as polymer-bonded composites [27], it is necessary to characterize and model their mechanical response in different loading regimes, including high strain rate, large strain deformation. However, it can be very challenging to perform high strain rate characterization of soft materials such as this, owing to issues of weak signal transmission, stress non-equilibrium, and inertial effects being significant compared to material strength [28–31]. Recent studies have shown that it is possible to achieve reliable insights into the high strain rate response of many properties, even at large strains, by a combination of careful experimentation and implementation of time-temperature superposition (TTS) as part of the data interpretation [32–34].

This paper provides an thorough exploration of the mechanical properties of a relatively low molecular weight, supramolecular polyurethane (SPU) which demonstrates healable characteristics [8]. The rheological and morphological properties were characterized along with the large strain compressive response, and a viscoelastic softening model was developed to describe the mechanical behaviour in monotonic and cyclic compression at low strain rates, monotonic compression from medium to high rates, as well as strain recovery at room temperature. We first characterized the consistency of molecularity and polymer morphology by executing ^{1}H nuclear magnetic resonance (NMR) spectroscopy and gel permeation chromatography (GPC) experiments. Repeatable processability of the SPU was confirmed by

both differential scanning calorimetry (DSC) measurements and rheometry. Further rheological analysis under controlled thermal cycles explored the dependence on the rate of change of temperature, which was described using an Arrhenius based model. There was good consistency between data from DSC, small angle X-ray scattering (SAXS) and large strain compression experiments. In order to model the compressive response, fundamental viscoelastic characterization was first obtained from a dataset assembled from rheological analysis and DMA experiments in which isothermal frequency sweeps were performed over a wide range of temperatures. The time-temperature superposition (TTS) principle was applied to produce a master curve, fitting into a Prony series to produce a generalized viscoelastic model describing small strain behaviour. To capture the large strain response over a wide range of strain rates, an additional characteristic dashpot and spring were combined with the generalized Maxwell model to allow strain softening and recovery to be modelled, respectively. This viscoelastic softening model was implemented in Simscape (MATLAB® & Simulink®), and calibrated using compression experiments at varying strain rates from 10^{-3} to 40 s^{-1}; it was then used to predict the results of high strain rate experiments up to 1220 s^{-1}. The geometric (strain) recovery during low-rate cyclic compression tests at room temperature was also incorporated into the model implementation.

2 Material and background characterisation

2.1 Synthesis of SPU and characterization methods

Thermoplastic polyurethanes are a class of phase-separated block co-polymer, formed by soft and hard segments, with varying ratios by mass. The desired material was synthesized as described previously [8][18]. Firstly, a hydrophobic polyol, namely Krasol™ HLBH-P2000, was reacted with methylene diphenyl diisocyanate (4,4'-MDI) at 80 °C for three hours to afford a prepolymer featuring isocyanate terminals. A hydrogen bonding motif, 4-(2-aminoethyl)morpholine, was then added to the prepolymer to install the end-groups via urea bond formation and afford the desired polyurethane as shown in *Figure 1*. The polyurethane was designed to permit hydrogen bonding interactions for network self-assembly, consequently achieving a healing capability at readily accessed temperatures around 37 °C [8]. ^{1}H NMR spectroscopy was first used to confirm the synthesis. ^{13}C NMR spectroscopy also corroborated the establishment of urea (156.2 ppm) and urethane (153.8 ppm) linkages in the supramolecular polymer. As an additional conformation of the formation of urethane/urea linkages in the polyurethane, infra-red spectroscopy revealed the complete consumption of isocyanates functionalities as observed by the disappearance of the vibration at 2270 cm^{-1}. Furthermore, new absorbances at 1642 cm^{-1} and 1706 cm^{-1} were attributed to the carbonyl stretches in the newly formed urea and urethane bonds, respectively. GPC analysis was conducted to confirm the extent of chain extension in the polyurethane, with an average of 2 hydrogenated poly(butadiene) residues per supramolecular polymer (M_n = 9100 g mol^{-1}).

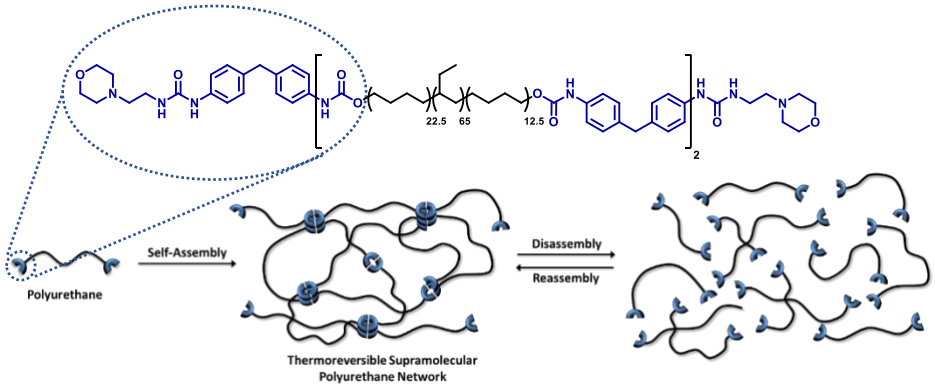

Figure 1: Chemical structure of the supramolecular polyurethane, featuring urea morpholine end groups, used in this study and a schematic illustration of formation and dissociation of the polymer network when an appropriate stimulus, such as heat, is applied

In order to perform the experimental program reported herein, samples of polymer were repeatedly re-melted and re-cast. This gave the requirement and opportunity to assess their stability. 'Raw' samples were produced first, by solution casting from THF into PTFE moulds. The samples were dried at room temperature overnight before drying at 80 °C under vacuum. To produce heat-treated specimens, this material was heated to 80 °C at 2 °C min^{-1} in an oven, and then cooled in air, in water, or under temperature-controlled cooling rates of 2 °C min^{-1} and 10 °C min^{-1}. Temperature profiles were measured using thermocouples embedded into one of the samples within the mould. Typical cooling curves for the air and water-cooled specimens are shown in Supplementary Information (SI), *Figure SI 1*. Samples that had each undergone four thermal treatments ('repetitive' specimens) were compared to 'raw' specimens and specimens that had undergone a single thermal treatment ('single' specimens). Spectroscopic and thermal analysis were carried out in order to identify whether any degradation had taken place via modification of the polymer backbone [35], or cross-linking [36][37] of the urethane or urea linkages. This allowed for the determination of whether disruption to the supramolecular network and polymer backbone had occurred over time. Finally, DSC, rheometry and SAXS experiments were performed in order to confirm that the order and assembly of the SPU network had not altered.

2.2 Molecular characterization

^{1}H NMR spectroscopy was conducted to examine the stability of the SPU under different processing conditions (*Figure 2*). Samples that had undergone thermal treatment were compared to the raw material and revealed no significant difference in chemical shifts or integration of key resonances. The successful synthesis of the SPU was first confirmed by which revealed a resonance at 4.16 ppm, characteristic of methylene residues adjacent to newly formed urethanes in the polymer backbone. Furthermore, the decoration of the pre-polymer with the hydrogen bonding motif was confirmed by the triplet at 3.33 ppm. This triplet was assigned to the methylene residue adjacent to the newly formed urea motif within the hydrogen bonding end-groups. The resonance at 4.16 ppm and 3.33 ppm corresponding to the methylene residue adjacent to urethanes and urea moieties, respectively, were unchanged after thermal processing, indicating that the polymer backbone remained intact. Importantly, the integration ratio between end-group resonances and the polymer backbone remained constant after thermal processing when compared to the raw material, demonstrating no alteration to the composition of the polymer network. Furthermore, no additional, new signals were observed in the ^{1}H NMR spectra for any samples after treatment, again demonstrating that the polymers were stable to the thermal processing conditions.

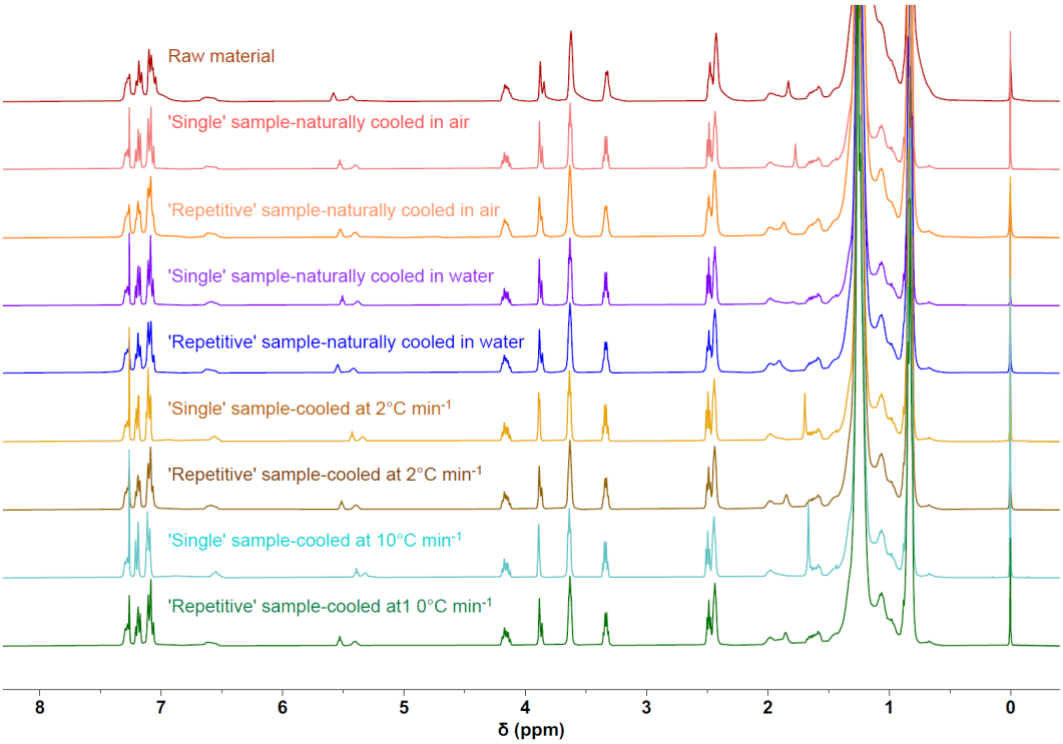

Figure 2: ^{1}H NMR spectroscopic data for SPU specimens following different thermal processing regimes, using air-cooling, water-cooling, or controlled cooling rates.

To further monitor the stability of the SPU under the thermal processing conditions described above, GPC experiments were undertaken to explore any changes in molecular weight (*Figure 3)*. In good agreement with the data collected by ^{1}H NMR spectroscopy, GPC analysis demonstrated no significant difference in the molecular weight of the materials after processing (M_n between 8650 g mol^{-1} and 8800 g mol^{-1}) compared to the raw material (8750 g mol^{-1}) as revealed by the multi-modal signals at retention times between 13 and 16.5 minutes. Furthermore, the polydispersity of all samples before and after processing was relatively narrow (Đ = 1.45), further revealing that no trans-urethanation had occurred [35].

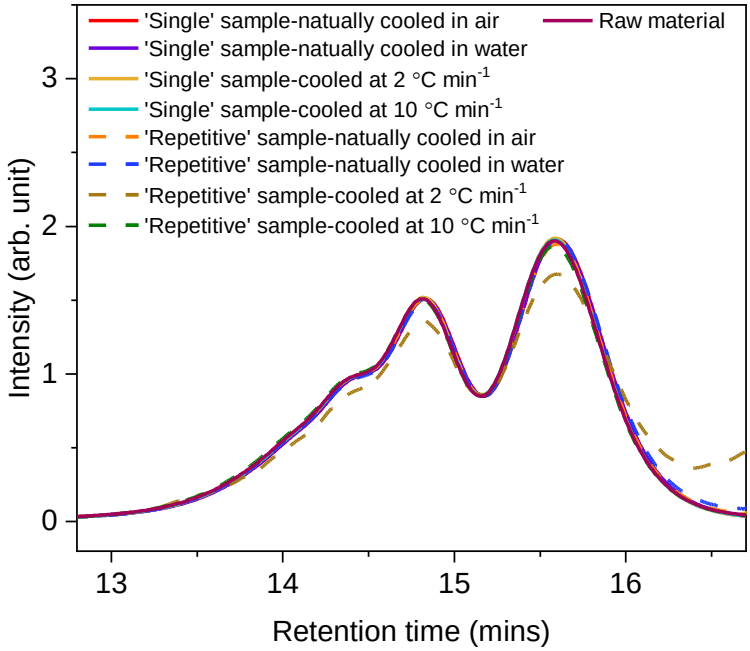

Figure 3: GPC results for three types of SPU specimens: 'raw', 'single' and 'repetitive', demonstrating that the molecular weights do not change with repeated processing.

2.3 Thermal Characterisation

DSC was used to examine the thermal properties of the material, focusing on the effect of different cooling rates, *Figure 4*. A single 'raw' specimen was taken and first cooled to -80 °C at 1 °C min^{-1}; after a 5-minute hold at -80 °C, a constant heating rate of 5 °C min^{-1} was applied until the temperature reached 90 °C, at which temperature the specimen was again held for 5 minutes. The specimen was subjected four cycles of cooling treatments from 90 to -20 °C, at different rates, each followed by heating at 5 °C min^{-1}. Full experimental data from three specimens can be viewed in the SI, *Figures SI 2-4*; *Figure SI 5* shows the consistency between heat flow data in the different cooling loops.

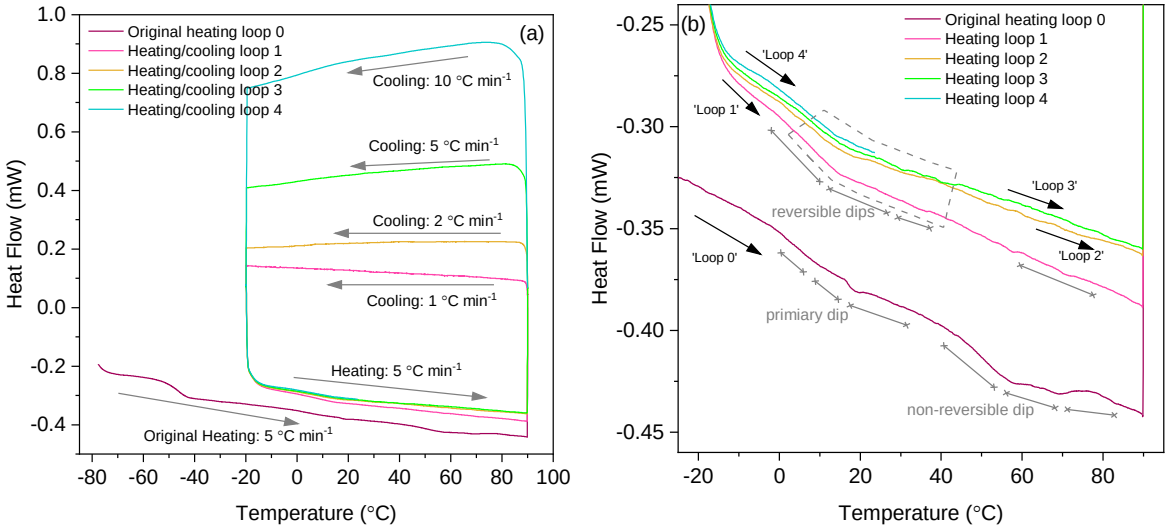

Figure 4: DSC experiments with different cooling rates performed on an initially cast specimen (a) measured heat flow for the different heating and cooling loops (b) detail of heating loops.

The DSC experiments revealed a glass transition at approximately -45 °C, which is the T_g of the soft domain within the micro-phase separated polymer. A second endothermic transition at around 20 °C was also observed, which may be associated with dissociation of the thermo-reversible supramolecular structure: this is repeated in all of the cycles. In the first heating, an additional broad endothermic dip was observed starting at 40 °C. This was not observed in subsequent cycles, and may be associated with phase separation within the cast material which has insufficient time to reform equilibrium in subsequent loops given the cooling and heating rates imposed [24]; evidence of an additional structure in the 'raw' specimens is shown in the SAXS data below.

2.4 Structural Characterisation

Small-angle X-ray scattering (SAXS), was performed to examine the nanoscale structure resulting from different cooling rates. SAXS was executed on both 'raw' and 'single' specimens, results are shown in *Figure 5*. All SPUs exhibited a typical micro-phase separated morphology as confirmed by the Bragg peak centered at 0.016 $Å^{-1}$, which arises from immiscibility of the polar hard (self-assembling) and apolar soft (polymer backbone) domains [8]. Additionally, the raw material exhibited a slight shallower SAXS profile compared to the

processed polymers at high q values (0.011-0.014 $Å^{-1}$) as a result of a potentially modified micro-phase separation. This may further corroborate the existence of kinetically trapped phase separation, as observed by DSC measurements. Furthermore, the SAXS profiles also possess a reflection centered at 0.061 $Å^{-1}$. This second order SAXS peak ($q\sqrt{3}$) corresponded to hexagonal packing of cylinders within the micro-domains as a result of association of the urethane-urea motifs which allowed to form without disruption. Again, no significant differences were observed in SAXS profiles of the materials post treatment demonstrating that the polymer was stable over the different cooling regimes reported.

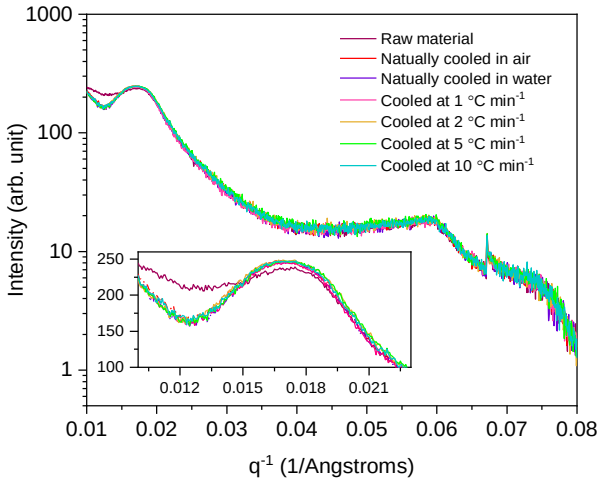

Figure 5: SAXS data obtained at 25 °C for 'raw' material, and 'single' SPU specimens prepared using different thermal processing regimes. All samples experienced a heating rate of 2 °C min^{-1} to a temperature of 80 °C before being cooled in air, in water or at controlled rates between 1 and 10 °C min^{-1}.

2.5 Effect of cooling on mechanical response

In addition, compression experiments were performed on water and air cooled specimens; temperature profiles can be viewed in *Figure SI 1*. The compression data, *Figure 6*, reveal that the material can be re-processed multiple times without degradation of initial stiffnesses, although small differences in behaviour were observed at large strains. This is consistent with the data presented above, in which the results were not affected by processing thermal cycles.

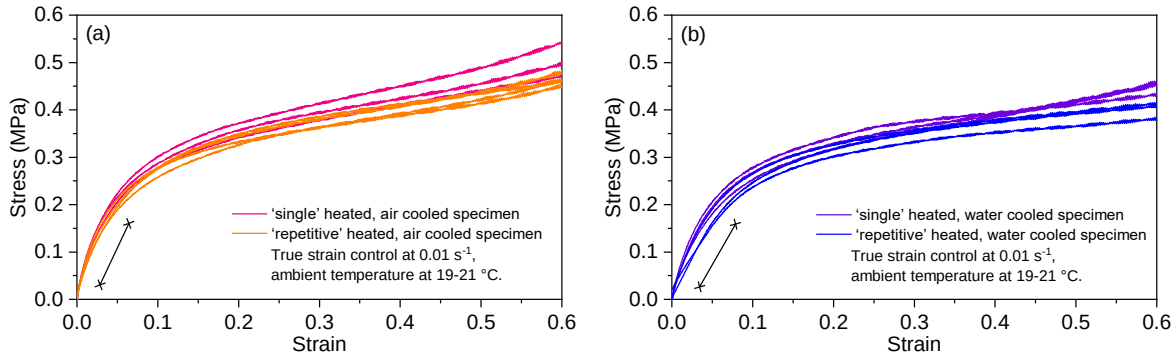

Figure 6: Stress-strain relationships in (a) air- and (b) water-cooled specimens under compression: 'single' specimens have undergone a single thermal treatment, while 'repetitive' specimen received four thermal treatments. The compression were performed at ambient temperature between 19-21 °C, differences between the curves might be due to temperature variations.

2.6 Rheological characterization

Rheological analysis was conducted to probe the mechanical properties of the materials, and their dependence on temperature and heating rate; data from this analysis were also used to populate later models of this behaviour. Test specimens were made by first melting the pristine solution cast (raw) material, and then casting a disk specimen of 20 mm diameter and 1.5 mm thickness using a PTFE mould (similar to the one in *Figure SI 21*); the density was measured as 950 kg m^{-3} and Poisson's ratio is 0.49. Rheometry experiments were performed under a constant oscillatory deformation at 1 Hz, with a 0.1 % shear strain amplitude. Before starting each experiment, the specimen was heated to 80 °C in order to ensure good contact between the specimen and plate. Two series of experiments were initially performed to investigate the effect of heating rate and cooling rate on the mechanical performance of the supramolecular polyurethane: in the first series, the specimens were heated from 20 to 90 °C at five different heating rates, before cooling at a constant 2 °C min^{-1}; in the second, the heating rate was fixed at 2 °C min^{-1} but different cooling rates were employed. In both cases, output data, including moduli and contact force were recorded.

Analysis of rheology data, *Figure 7*, showed that the higher heating rates gave rise to a higher modulus on heating, but that there was no effect on the properties measured during the

subsequent cooling regimes; similarly, higher cooling rates gave a lower modulus on cooling, but have no effect on the properties during subsequent heating. This is consistent with the DSC data, and SAXS analysis. Further rheological experiments were performed to confirm repeatability of the data from different cycles, and to confirm that the results obtained were not affected by previous cycles (*Figure SI 6*). Overall, the data demonstrate the reversibility of material properties, and support the reusability of the material. They also indicate that there is a time dependence in the evolution of the polymer structure, and hence the mechanical response, but that the time taken for the reversal of the temperature ramp at room temperature is sufficient for the subsequent ramp to be unaffected.

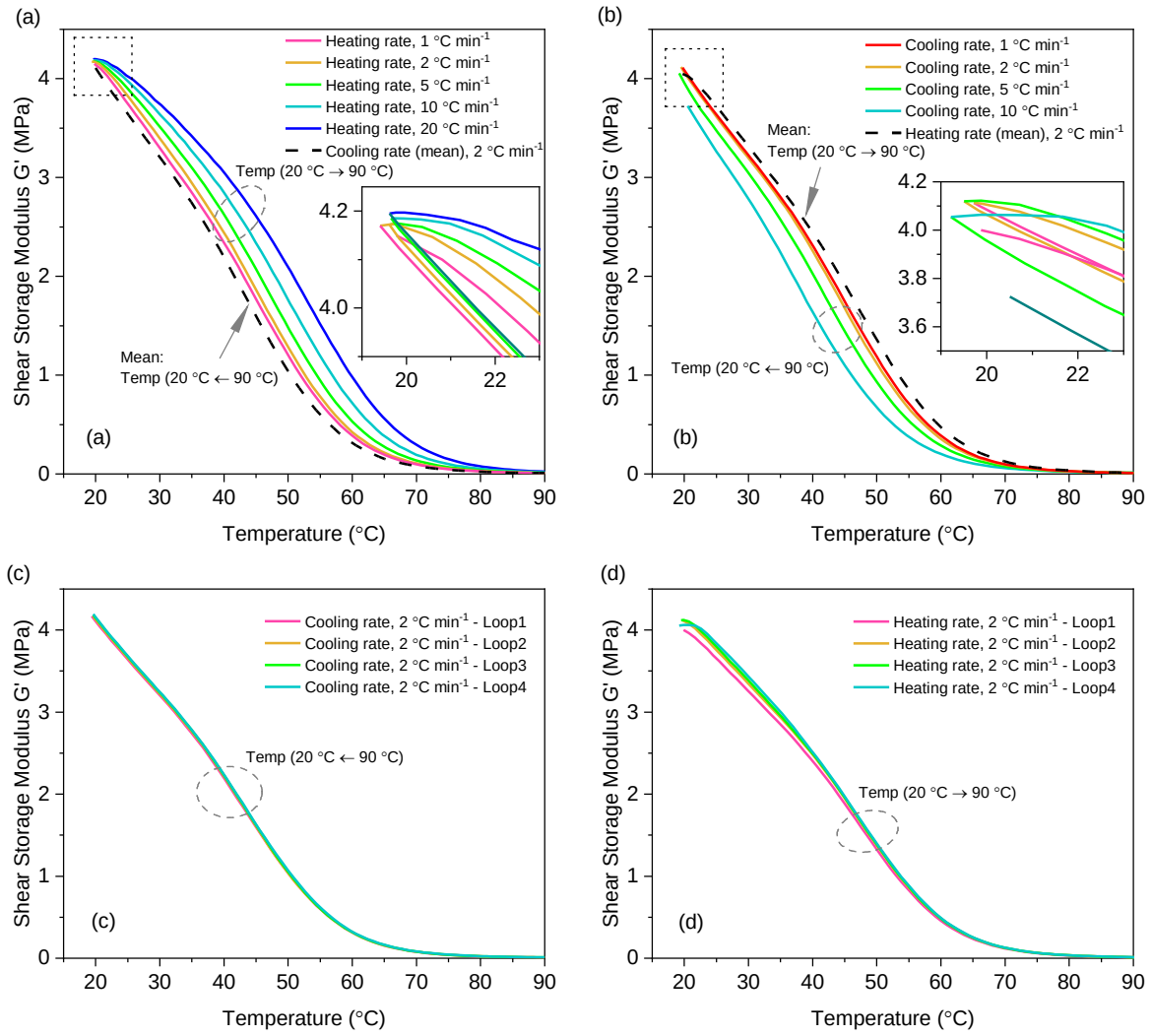

Figure 7: Rheological analysis at different (a) heating rates or (b) cooling rates of 1, 2, 5, 10, 20 °C min^{-1}. Mean data for the cooling and heating portions of the loops (at 2 °C min^{-1}) are also shown. The full sets of results from cooling and heating, respectively, are shown in (c) and

(d). These data also show that processing at different rates does not affect the subsequent properties. Oscillation frequency 1 Hz and amplitude 0.1%.

2.7 Models for rheological characterization

Two simplified models were used to characterize the effects of heating or cooling on observed material properties. The first model, the 'shift method', was based on the observation that data from different heating and cooling rates had a similar shape through the experiment, but were simply offset from one another. This led to the concept that any modulus-temperature profile at a certain heating or cooling rate might be predicted using data obtained from a reference rate. The analytical formulation of this model is introduced in the SI, with implementation shown in *Figures SI 7-8*. The second model used a differential equation based on an Arrhenius formation including both time and temperature variables, to calculate the unit moduli on each unit temperature rate. These methods were chosen as they are both commonly used to describe time-temperature equivalence in polymers. The appropriate parameters were found by fitting to the experimental data. Here, the Arrhenius model is described briefly, more detail about both models may be found in the SI.

The second model explicitly captures the evolution of modulus with time and temperature using an Arrhenius equation to model the temperature effect on the rate at which the polymer structure evolves. This relationship is often applied to the physical interpretation of kinetic transformations induced by thermal process [38][39]. The model describes the rate of change of modulus with respect to temperature according to

$$\frac{dG}{dt} = r_0[G - G_{ref}(T)]e^{-\frac{U}{kT}} \qquad \textit{Eq. (1)}$$

where G is the current modulus output by the rheometer; $G_{ref}(T)$ is a temperature-dependent reference 'long term' modulus to which the current modulus evolves; r_0 and U are parameters to be calibrated using the empirical data; T is the absolute temperature; and k is the Boltzmann constant, equal to 1.3806×10^{-23} J K^{-1}. In practice, G_{ref} was assumed to be the modulus-temperature profile produced by averaging the cooling and heating curves at 2 °C min^{-1}. *Figure*

8, shows modulus curves on heating and cooling, as produced by the model, using parameters of r_0 = 2 s^{-1} and U/k = 1312 K. It is noted that here the measured time-temperature profiles (*Figure SI 10*) were used, allowing the model to account for the changes in heating and cooling rate through the experiment, thus representing an advantage of this approach.

Further validation of the model, via comparison to other experiments to verify its capacity and applicability is provided in the Supplementary Information, *Figures SI 12-16*.

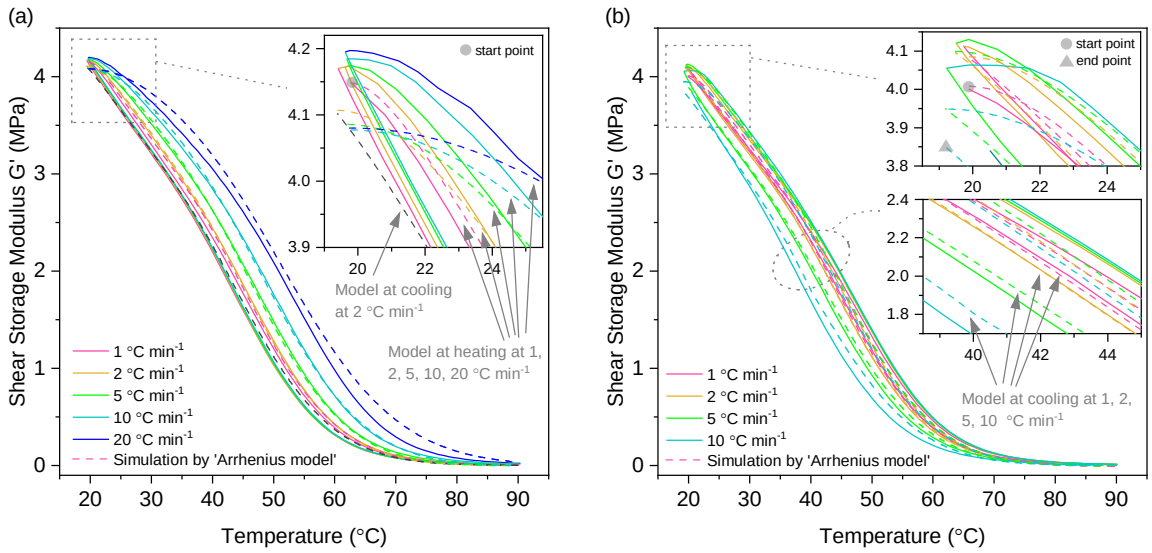

Figure 8: Application of the Arrhenius equation based model to (a) heating and (b) cooling rates of 1, 2, 5, 10, 20 °C min^{-1}. The reference curve was the average of cooling and heating at 2 °C min^{-1}, representing the temperature rate $\dot{T} \rightarrow 0$. The experimental temperature profiles and model parameters of r_0=2 s^{-1} and U/k=1312 K were used. Oscillation frequency 1 Hz and amplitude 0.1%.

3 Dynamic Mechanical Analysis and production of Master Curves

In order to understand and model the data obtained from monotonic compression testing reported in later sections, thermo-mechanical analysis of the specimens was performed using Rheometry, as described above, and DMA. Each of these systems is able to characterize a different regime of material behaviour: rheometry for elevated temperatures where the material has low modulus, and DMA for low temperatures, for which the stiffness is higher. The empirical behaviour of thermoplastic elastomers between the rubbery and glassy states has the well-known time-temperature equivalence [40]. Making use of this, master curves of the behaviour as a function of frequency at different temperatures were produced from the experimental data in a manner consistent with the later modelling strategy. The rheometer sample was first prepared by melting at 80 °C, and air cooling in a PTFE mould to produce specimens of diameter 20 mm and thickness 1.5 mm. Once inserted in the rheometer, the specimen was again heated to 80 °C and cooled back to room temperature (at 2 °C min^{-1} for heating and cooling) to ensure full contact with the measurement plates and removal of potential residual stress. Isothermal frequency sweeps (1-100 Hz with 100 measurement points) were then performed at 10 °C temperature intervals from -20 to 80 °C at 0.1 % shear strain.

For the DMA experiments, rectangular samples (5 × 20 mm, thickness 1.2 mm) made in the same manner were tested in a DMA machine (Q800, TA Instruments) in the tensile mode. Isothermal frequency sweeps were again performed, but at 5 °C temperature intervals from -60 to 30 °C, at 0.05 % strain and with 20 frequencies between 1 and 100 Hz. In these DMA experiments, however, the specimen was observed to start exhibiting significant permanent elongation, ether yielding or creep, when the temperature was above 15 °C. Conversely, the rheometer is not able to produce accurate data at low temperatures, below -10 °C this is shown in *Figure 9* and *Figure SI 17*. Therefore, the experimental data from DMA and rheological analysis were combined together to produce a single master curve, taking advantage of the ability to produce overlapping data, in *Figure 10*; the shift factors and a Master Curve for *E''*, are given in *Figure SI 18*. The

shift factors can themselves be fitted by the well-known Williams-Landel-Ferry (WLF) equation [41],

$$\log a_T = -\frac{C_1(T - T_{ref})}{C_2 + (T - T_{ref})} \qquad \textit{Eq. (2)}$$

where T_{ref} is a reference temperature, and C_1 and C_2 are constants fitted to the data. Further, the master curve can be fitted by a Prony series

$$E(t) = E(0)\left[1 - \sum_{i=1}^{M} \frac{E_i}{E(0)}\left(1 - e^{-t/\tau_i}\right)\right] \qquad \textit{Eq. (3)}$$

where $E(0)$ is the instantaneous elastic modulus in the time domain, and the values of E_i and $\tau_i = \eta_i / E_i$ are fit to the experimental data. These parameters can also be used to express the storage and loss moduli as functions of frequency using

$$E'(\omega) = E_0 + \sum_{i=1}^{M} E_i \frac{\tau_i^2 \omega^2}{1 + \tau_i^2 \omega^2} \qquad \textit{Eq. (4)}$$

$$E''(\omega) = \sum_{i=1}^{M} E_i \frac{\tau_i \omega}{1 + \tau_i^2 \omega^2} \qquad \textit{Eq. (5)}$$

where ω is the applied frequency. Here, E' and E'' are defined as the real and imaginary parts of the complex moduli during cyclic loading. In this case, the Alfrey Approximation [42] was used to parameterize the Prony series, which was then applied in the model described in the next section; the parameters obtained are given in *Tables SI 1 to 3* at different temperatures, the Prony series at different temperatures are also shown in *Figure SI 19*.

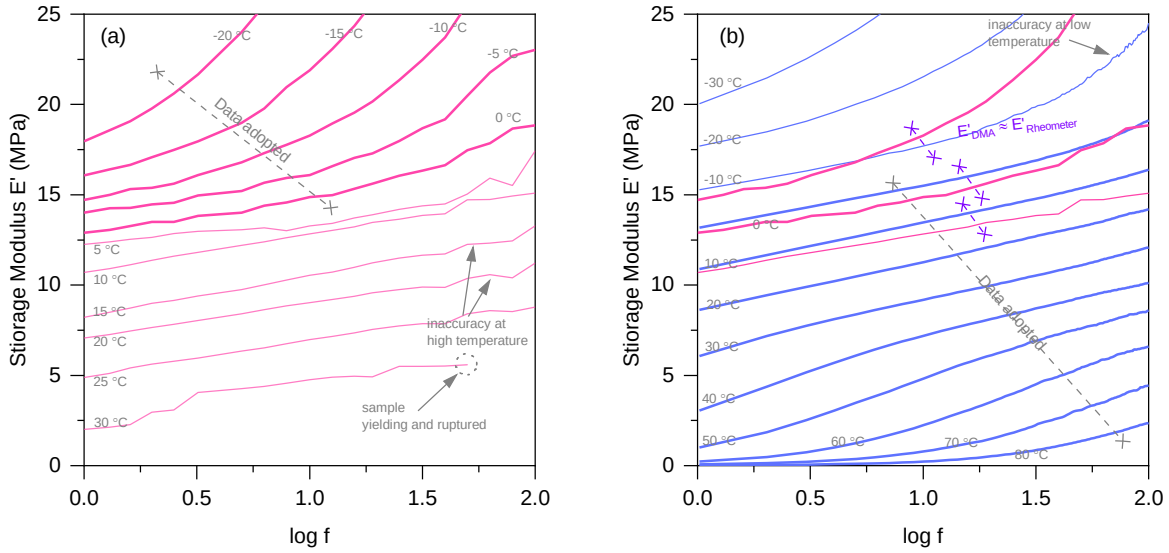

Figure 9: (a) DMA data showing isothermal frequency sweeps at different temperatures. The DMA performs well from -60 to 30 °C but inaccuracies are apparent above 10 °C. (b) Rheometer data are accurate at higher temperatures but not below -10 °C. Here, DMA data at -10, 0 and 10 °C are overlaid to show the consistency between these two techniques.

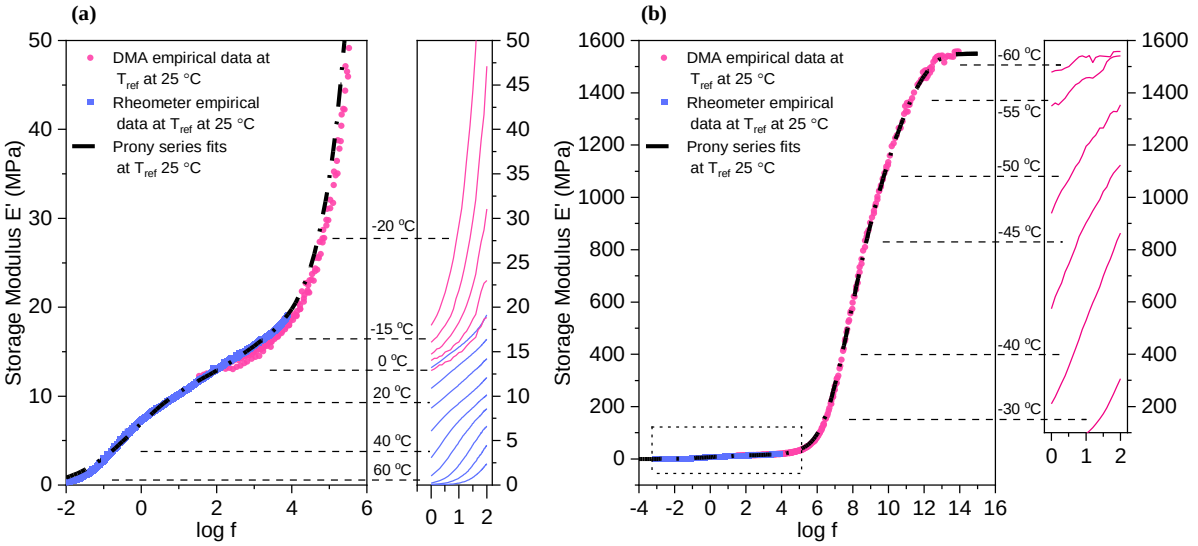

Figure 10: (a) and (b) A continuous master curve of E' vs. log f generated by applying TTS to E' vs. log f curves at different temperatures from the rheometer and DMA. In particular, (a) shows the consistency between the two sets of data. A Prony series was fitted to the storage modulus profile in (b) using the full range of frequencies.

4 Viscoelastic Softening Model

Phenomenological models of polymers are commonly used to describe viscoelastic, viscoplastic, and softening behaviour [43–46]. These models often use combinations of Hookean springs and Newtonian dashpots to describe the empirical behaviour [46–50]. A simple model, *Figure 11*, is proposed here and calibrated using thermo-mechanical data as well as compression tests. Here, the generalized Maxwell model is used to express the fundamental viscoelasticity, calibrated by using the Prony series fit to the rheometer and DMA data as described above; there is an additional dashpot (η^*) added to allow softening at larger strains, observed in the compressive data; finally, an external spring (E^*) captures strain recovery observed upon removal of load. In order to aid the fitting to the experimental data, two forms of the dashpot were used: η^*_{linear}, in which the viscosity was independent of stress level, and $\eta^*_{\textit{non}\text{linear}}$, in which there was stress dependence. The entire model was constructed in Simscape (Simulink, Matlab), shown schematically in *Figure SI 20*. In order to calibrate the model, quasi-static compression experiments were performed; the model was later tested against data obtained at higher strain rates. The quasi-static experiments were executed in a commercial screw-driven testing machine (Instron 5982). Test samples of diameter 6.3 mm and height 7.3 mm were cast in a PTFE mould (*see Figure SI 21*) at 80 °C, using the same approach introduced in the rheometry section, and air-cooled to room temperature. Experiments were conducted at strain rates of 0.001, 0.005, 0.01, 0.05, 0.1 and 0.5 s^{-1}; force was recorded using a load cell and strain calculated from local measurements of the axial displacement using an extensometer attached to the loading platens: the experiments were performed at constant true strain rate. After the test, the zero-stress strain recovery was recorded against time.

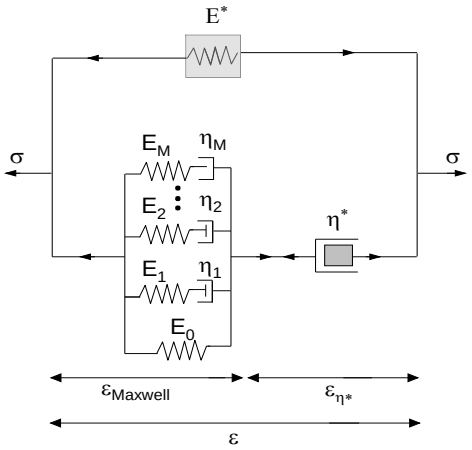

Figure 11: Schematic of the viscoelastic softening model. The model combines springs and dashpots described by the Prony series, an additional dashpot η^* and a recovery spring E^*.

The characterization of the dashpot (η^*) and spring (E^*) is provided in *Figure 12*. The strain rate-controlled model was implemented to compute stress-strain responses at different strain rates. The values of η^*_{linear} were defined at each strain rate by optimizing the model to the experimental data. From the outputs, it was observed the model stress-strain response started to flatten around strain 0.6, showing that the dashpot is fully activated. By inputting the initial linear value of η^*_{linear} to match the empirical strain-stress curves (shown later in *Section 5*), the value of stress was determined when $\varepsilon = 0.6$. These values of η^*_{linear} and stress enabled construction of a linear relationship of log η^* against log σ. This implied a relationship of the form

$$\frac{d\sigma}{d\dot{\varepsilon}} = 10^{\beta} \cdot \sigma^{\alpha} \qquad \textit{Eq. (6)}$$

where α and β are fitting parameters for the linear relationship. Applying the boundary condition: $\sigma(t=0) = 0$, allows a relationship to be derived between stress and strain rate by in order to characterize the dashpot:

$$\sigma = (\chi\dot{\varepsilon})^{\delta} \qquad \textit{Eq. (7)}$$

where χ and δ are determined by solving the differential equation (ODE) in *Eq. 7*.

In the Simulink model, η^*_{linear} can be simply represented by a standard linear dashpot; while for $\eta^*_{nonlinear}$, the behaviour was described using a 'Lookup Table'. This was implemented

by fitting well-selected dispersed values along the plot given by the ODE solution. In practice, larger numbers of sampling points were taken at low strain rates, with more dispersed points up to 40 s^{-1}. It is noted that the strain rates experienced in this dashpot are small even when the overall strain rate is high. Now, both η^*_{linear} and $\eta^*_{nonlinear}$ can be inserted into the Simscape model allowing simulation of experiments over the full range of strain rates, as demonstrated in later sections.

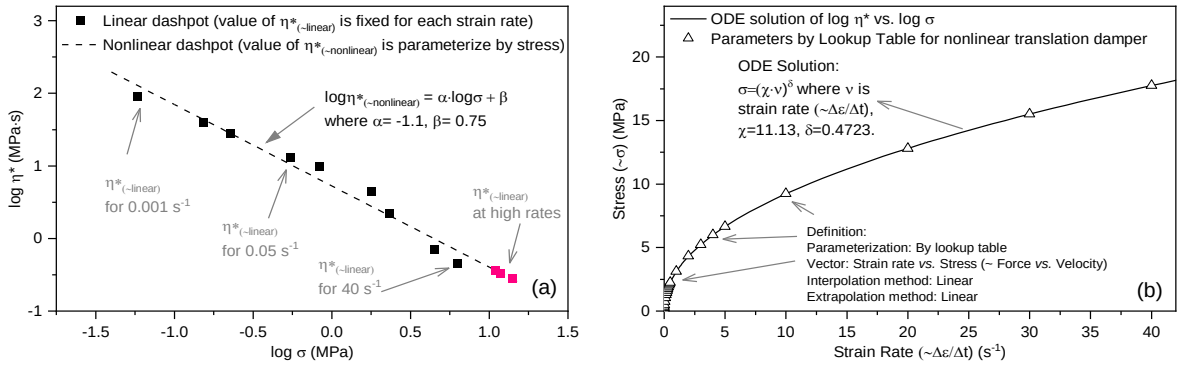

Figure 12: (a) A series of linear dashpots was first fitted to the experimental data, the logarithms of the fitted viscosities were found to be linear in log(applied stress), described by the function given and extrapolated to high strain rates. (b) The character of the non-linear dashpot was determined by finding the solution to the ODE formed for $\eta*$ against σ; this was then sampled at the points shown to produce a lookup table for the model.

The value of the spring, E^*, was then determined. Having derived the stress-strain relationship for loading, the stress history was re-inputted back to the Simscape model using stress-control (*Figure 11*). To simulate the recovery after compression, a zero-stress period was added after the loading history to form a full representation of the specimen history, including loading, unloading and recovery. This was done to avoid complications when switching between strain rate and stress control. An appropriate value of E^* (= 0.85 kPa) was fit by comparing the model output to empirical strain recovery data, shown in *Figure 13b*. All recovery experiments and simulations were performed at 25 °C and recovery data can be reviewed in *Figure SI 22 and Table SI 4*.

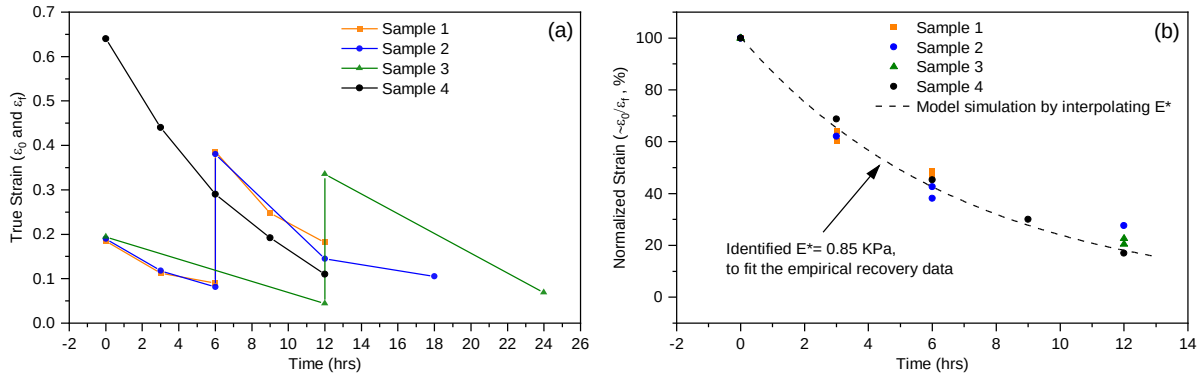

Figure 13: (a) A series of specimens were compressed to different strains, ε_f, (in experiments lasting a few minutes) and allowed to recover a period of a few hours before being reloaded, whilst the strain, ε_0, was monitored; some of the samples were then reloaded. (b) a value of E^* = 0.85 kPa allowed the model to capture the recovery history of a number of samples, including those loaded cyclically (1-3) or monotonically (4) to different strains. All experiments were executed at a temperature of 25 °C.

An example of a full set of model outputs for a monotonic loading is shown in *Figure 14*. The figure shows the stress-strain behaviour in the Maxwell components, identified spring E^* and the entire model, as well as the strain behaviour of the Maxwell model, identified dashpot $\eta^*_{nonlinear}$ and the whole model, on both short and long timescales.

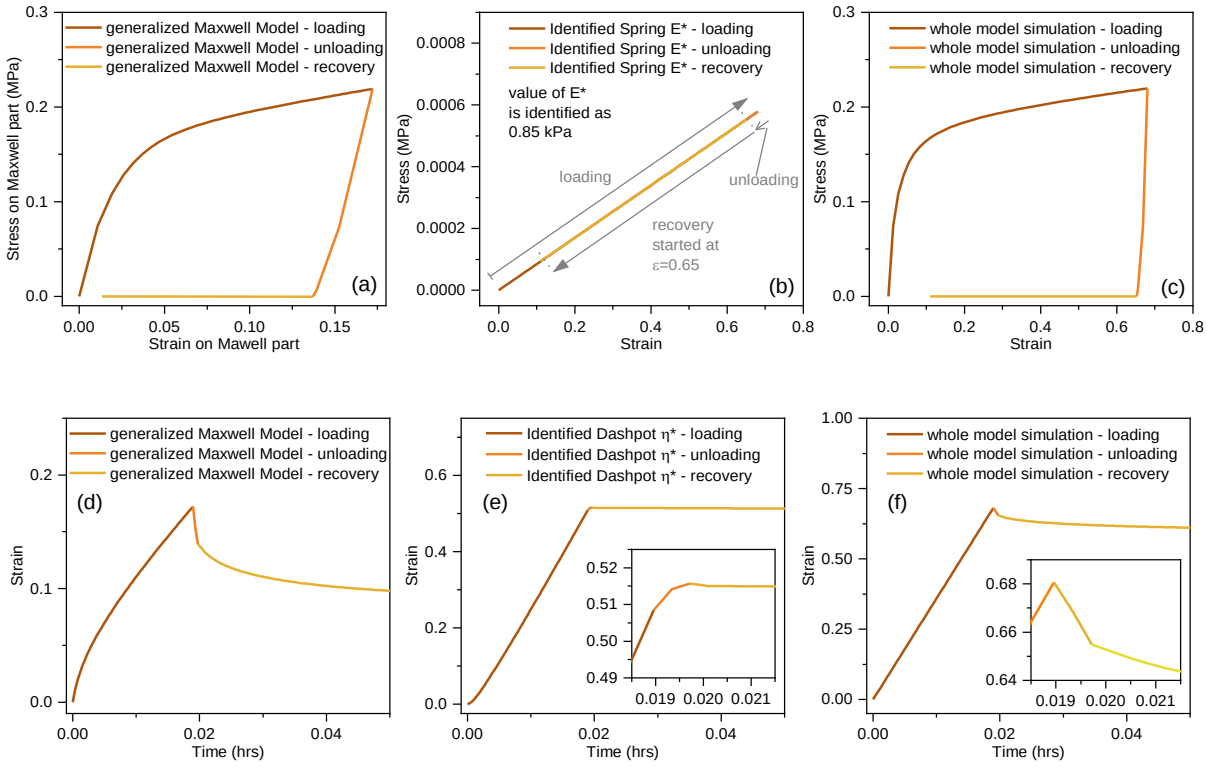

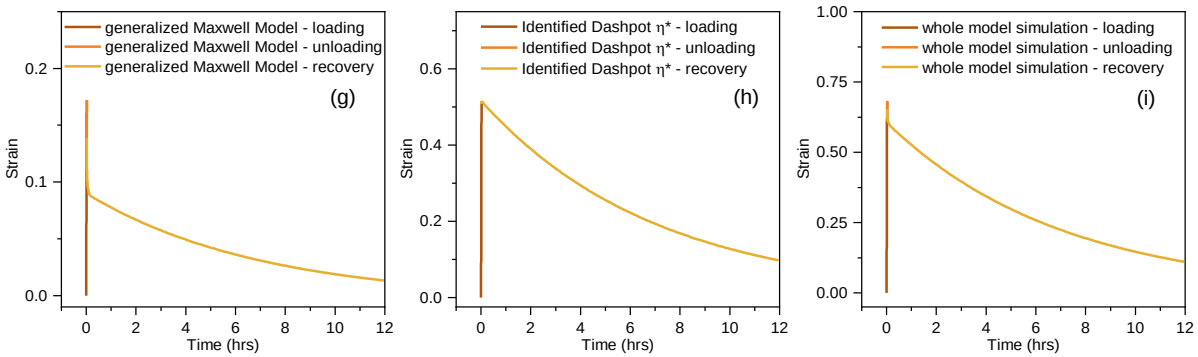

Figure 14: Model outputs for a sample compressed at 0.01 s^{-1}, 25 °C. The figure shows stress-strain relationships and strain time histories in different components of the model.

5 Application of Viscoelastic Softening Model

5.1 Model application at low-to-medium strain rates

Experiments were performed at a constant temperature of 25 °C but various strain rates: true strain rates of 0.001, 0.005, 0.01, 0.05, 0.1 and 0.5 s^{-1} using a commercial screw-driven testing machine (Instron), and true strain rates of 1.36, 11.5 and 40 s^{-1} using an in-house hydraulic system[1]. The samples had diameter 6.3 mm and thickness 7.3 mm. At least three samples were tested at each rate, the representative data was selected to show in this section. Full data can be viewed in *Figure SI 23* and *24*. The development of the model for loading and (for the lower strain rates) unloading is shown in *Figure 15, Figure 16* and *Figure 17*. The isolated generalized Maxwell model is shown in *Figure 15*, this model over-predicts the specimen response. Then the viscoelastic softening model was applied, *Figure 16* and *Figure 17* which show a comparison of implementations using η^{*}_{linear} and $\eta^{*}_{nonlinear}$: firstly the linear implementation, in which a constant viscosity value is fit to each experiment and then the nonlinear implementation, in which a global, stress-dependent $\eta^{*}_{nonlinear}$ is used. Both models are shown to well describe the experimental data. In particular, at strains below 0.08 the generalized Maxwell model has good agreement, showing that the Prony series derived from DMA and rheometry master curves are sufficient to capture this behaviour. At larger strains, the addition of the extra dashpot and spring allowed the model to describe both the softening (relative to the Maxwell model) and subsequent unloading. An example of the behaviour of the model components can be viewed in *Figure SI 26*. A discussion of recovery and cyclic loading will follow in *Section 6*.

[1] These strain rate may be related to the material relaxation frequencies in Figure 10 by assuming that the relevant frequency and strain rate are approximately equal. Whilst this is a simplification, it allows an understanding of the material regime of relevance in these experiments.

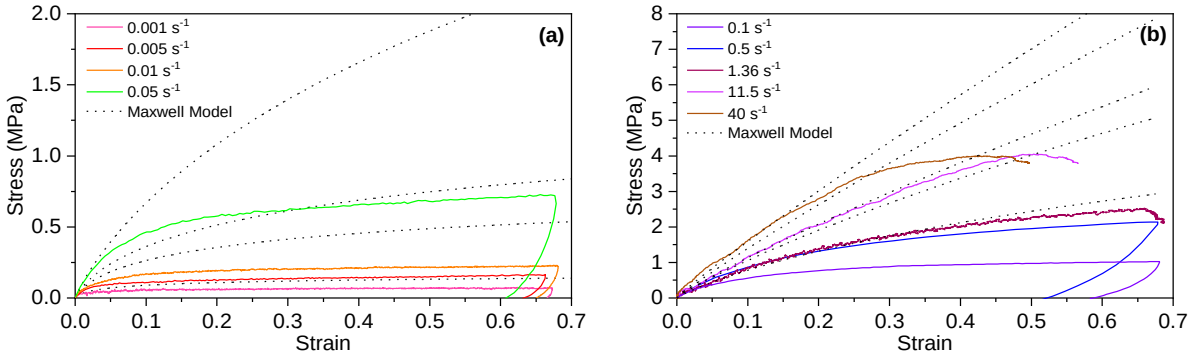

Figure 15: Isolated generalized Maxwell model compared to low and medium rate compression experiments, at a temperature of 25°C but varying strain rates.

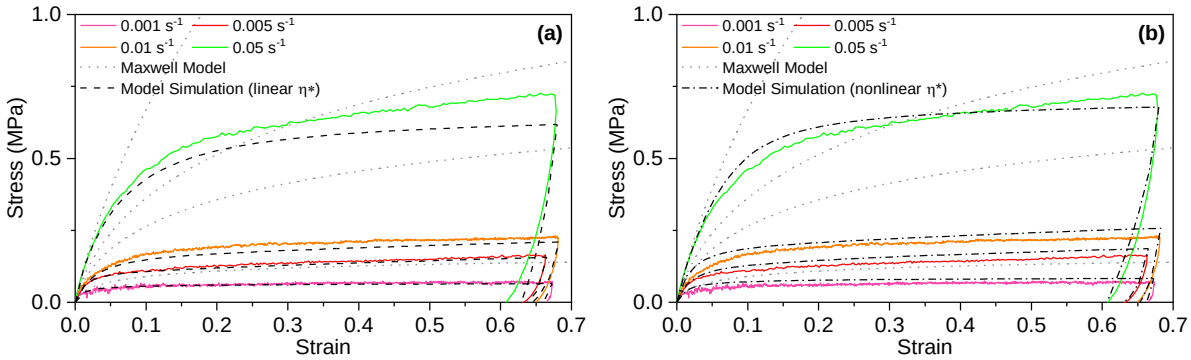

Figure 16: Viscoelastic softening model with linear dashpot η^*_{linear} (strain-rate dependent) and nonlinear dashpot $\eta^*_{nonlinear}$ (stress-dependent value), compared to low strain rate compression experiments, at a temperature of 25°C but varying strain rates.

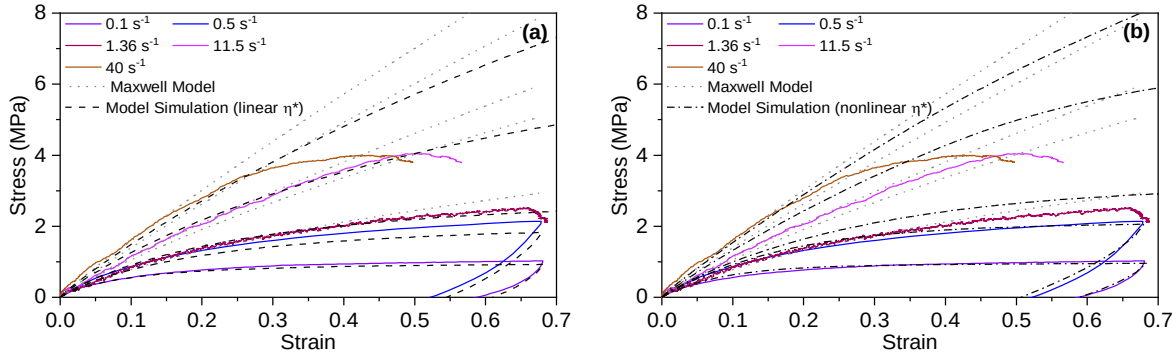

Figure 17: Viscoelastic softening model with linear dashpot η^*_{linear} (strain-rate dependent) and nonlinear dashpot $\eta^*_{nonlinear}$ (stress-dependent value), compared to low strain rate compression experiments, at a temperature of 25°C but varying strain rates.

5.2 Model application at high strain rates

The split Hopkinson bar (SHPB) technique is a standard methodology to study the high rate compression of polymers, as well as other materials [29]. In the experiments in this study, a cylindrical specimen was placed between the ends of two titanium alloy bars, *Figure 18*. A third striker bar is accelerated using pressurized gas into the incident bar. The subsequent impact creates an 'incident' stress wave which travels along the bar to the specimen. At the bar-specimen interface, some of the wave are reflected and some transmitted. The incident, reflected and transmitted waves were measured by strain gauges attached to the incident and transmission bars. These strain waves were used to calculate the deformation rate and force at the specimen interfaces, from which the corresponding true stress and true strain in the specimen were obtained. Since the stresses supported by this material are very low, a pair of bars instrumented with an additional pair of sensitive piezo-electric stress gauges, mounted at the specimen bar interfaces, was used for the specimen stress measurements [51].

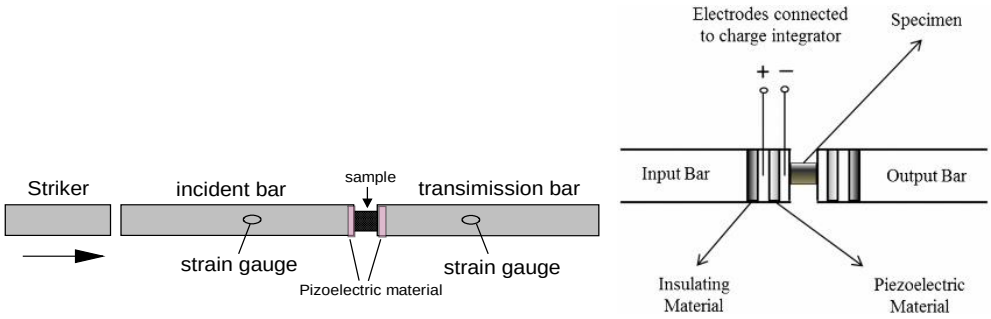

Figure 18: Experimental configuration for SHPB test [51]

Compression SHPB experiments up to 1220 s^{-1} were executed. Full experimental data can be reviewed in *Figure SI 25*. For these experiments, the environmental temperature was measured as 17 °C, so a new Prony series was generated by shifting the original master curve from 25 °C (shown in *Figure SI 19* and *Table SI 3*). The new master curve and new Prony series were then applied to the generalized viscoelastic Maxwell model to form the basic component of the softening model. The value of the additive dashpot and spring were consistent with those used in the previous section: the dashpot η^{*}_{linear} *and* $\eta^{*}_{nonlinear}$ were identified from

the previous extrapolation in *Figure 12*. A comparison of the model outputs and experimental data are shown in *Figure 19*. It is noted that the empirical temperature must be recorded accurately due to the temperature sensitivity of the material, see *Figure SI 28*.

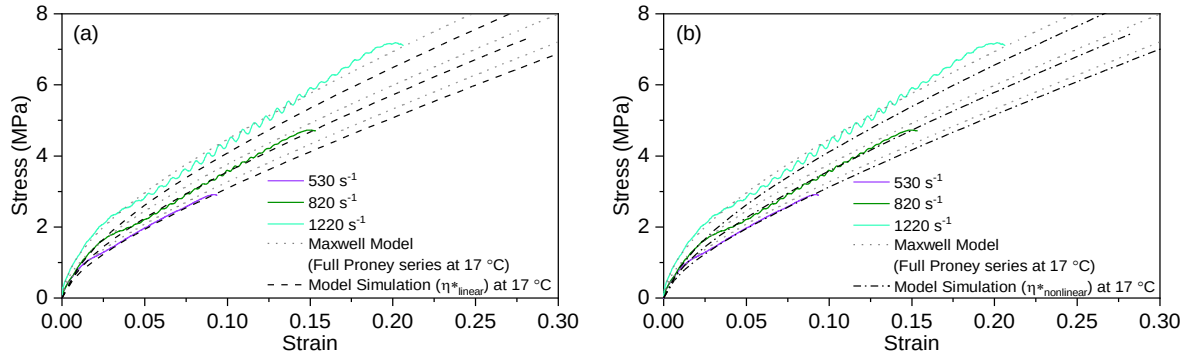

Figure 19: The high-strain rate compression experiments, at a temperature of 17 °C. The value of η^*_{linear} used was 0.47, 0.44, 0.36 for strain rates of 530, 820 and 1220 s^{-1}, obtained from the linear fitting in Figure 12a. The models using $\eta^*_{nonlinear}$ used the table derived in in Figure 12b. The stress-strain curves for the viscoelastic Maxwell model and the full model using the two identified dashpots are shown.

For these experiments, it was observed that the viscoelastic Maxwell model already provides good agreement with the empirical curves, whilst the addition of the viscoelastic softening improves this further (e.g. at 530 and 830 s^{-1}). At these strain rates the resistance of the dashpot to deformation is high, so it does not contribute significant additional strain. Further figures illustrating the stress and strain rate in the dashpot, and other model elements, are given in the *Figure SI 27*. Therefore, the softening model is a fully predictive methodology, which enables predict high rate behaviour from the master curve and low rate response.

The effect of specimen inertia must be taken into account when interpreting data from Hopkinson bar experiments. The rapid acceleration of the specimen produces extra stress measured in the system. In this case, the specimen is accelerated to the peak strain rate 1220 s^{-1} from rest. The specimen stress measured during a Hopkinson bar experiment through of the sum of stress components [52]:

$$\sigma_T = \sigma_M + \sigma_I + \sigma_F + \sigma_{other} \qquad \textit{Eq. (8)}$$

where σ_T is the stress measurement, σ_M is the material strength to be measured, σ_I is an enhancement owing to inertia, σ_F is an enhancement owing to friction and σ_{other} is the enhancement owing other effects that may be present.

The inertia-induced stress is calculated by [52–54]

$$\sigma_I = \rho\ddot{\varepsilon}\left(\frac{a^2}{8}-\frac{h^2}{6}\right)-\rho\dot{\varepsilon}^2\left(\frac{a^2}{16}+\frac{h^2}{6}\right)-\frac{\rho h\dot{v}}{2} \qquad \textit{Eq. (9)}$$

where ρ is the material density, $\dot{\varepsilon}$ and $\ddot{\varepsilon}$ are strain rate and strain acceleration, a = 4.9 mm is the radius, and h = 7.3 mm is the height, of this specimen, and v represents the speed of the output bar. The magnitude of this inertia stress is only 0.08 MPa at a strain rate of 1220 s^{-1}: the inertia effect is not significant in these experiments.

Another possible effect was the temperature rise owing to the conversion of mechanical work to heat. The high strain rate experiment is assumed to take place in adiabatic conditions as the duration is very short. Therefore any heat generated during the loading will be retained in the specimen, causing an increase in temperature which can be approximated, assuming that all the mechanical work done is converted to heat, by [55]

$$\Delta Q \approx \Delta W \rightarrow \int_0^{\varepsilon}\sigma d\varepsilon = \rho C_p \Delta T \qquad \textit{Eq. (10)}$$

$$\Delta T(\varepsilon) = \frac{\beta}{\rho C_p}\int_0^{\varepsilon}\sigma d\varepsilon \qquad \textit{Eq. (11)}$$

where ΔW is the work done, ΔQ is the heat generated, σ the true stress, ε the true strain, ρ = 950 kg m^{-3} the material density, C_p = 1850 J kg^{-1} K^{-1} the specific heat capacity at constant volume and ΔT the rise in temperature. Here, the heat capacity C_p is obtained from the DSC experiments. Using the assumption that $\beta \rightarrow 1$ for all the work is converted to heat, which is a significant over-estimate for these materials in which we have shown the that quasi-static loading is recoverable, this equation gives a temperature rise of only 0.4 °C at 0.2 strain in strain rate of 1220 s^{-1}, which only causes slight changes in the simulation results, shown in *Figure SI 29*.

6 Model application to strain recovery and cyclic loading

As described above, the spring E^* was calibrated to match the recovery of the specimens after leading. Once calibrated, this model was used to simulate cyclic experiments in which the specimen was loaded, unloaded, allowed to rest for 6 hours and then reloaded; an example is given in *Figure 20*. More information about the strain recovery in the different elements of the model is presented in *Figure 21*. The most important point to note here is that the same value of E^* successfully describes the behaviour of specimens loaded to different final strains.

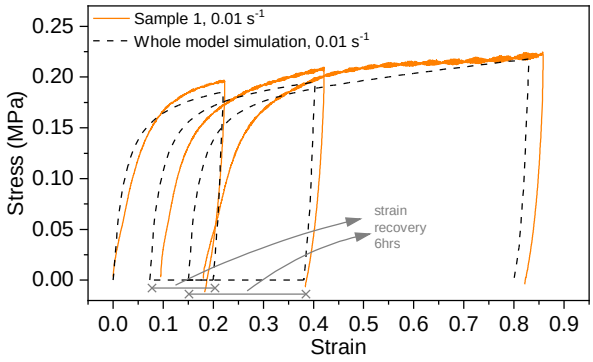

Figure 20: The viscoelastic softening model compared to a multi-cyclic compression experiment.

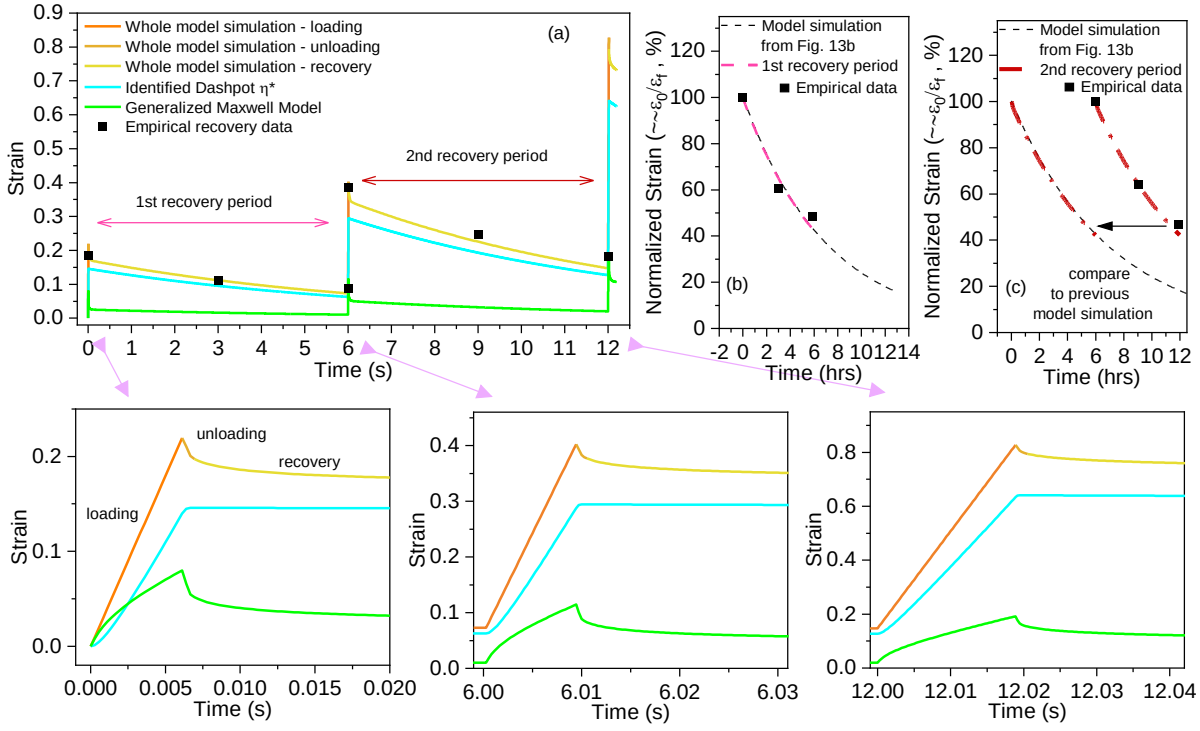

Figure 21: The viscoelastic softening model under stress-control (e.g. the zero-stress vs. time as input profile) to simulate the recovery process. The figures display (a) strain profiles of the

full model, dashpot and Maxwell elements. (b) The model simulation of first recovery and second recovery compared to the empirical data. The measured strain data are given in Table SI 4.

7 Conclusions

This paper presents data on the thermo-mechanical response of a supra-molecular polyurethane, and a simple model to capture this response. Structural characterization has been performed, which, combined with compression data on recycled specimens, show the reusability of the material over multiple cycles. Further, a simple model of the response during rheological characterization is presented, along with a model for the large strain behaviour which, in particular, is able to predict the high strain rate response

^{1}H NMR spectroscopy, GPC and DSC analysis have shown that the molecular architecture, molecular weight and intermolecular hydrogen bonding of the polymer were not affected by the cooling rate, showed little dependence on cooling rate during processing, and that there was no observable degradation when subjected to multiple heating and cooling cycles. DSC and SAXS analysis also demonstrate that, apart from an initial structure obtained during solution casting, the structure is thermo-reversible; this is also supported by cyclic rheological experiments. Considering the mechanical data, there is a small difference in the response of the material as a result of different cooling rates, as reflected in both the rheometry results and large strain compression data. Further work would be required to understand these changes. The variation in mechanical behaviour in the rheometer experiments was calibrated by two models: the 'shift method' and an Arrhenius based differential equation, in which it is important to consider the exact experimental temperature profile. The time-dependence of the mechanical properties are noted; however, it is also observed that the differences quickly disappear, and the differences observed during cooling do not affect the subsequent heating cycles.

In order to build the large strain mechanical model, characterization of time and temperature dependence was performed using both DMA and rheometry experiments. These data sets were combined to derive a master curve, which was described using a generalized Maxwell model and Prony series. Comparison of this model to large strain compression data

indicated that it was not able to capture the softening of the material, hence a modified viscoelastic model was developed using an additional dashpot to capture large strain response, and a spring for strain recovery. The model was first fit using linear dashpots with different values according to the loading rate; these were then replaced with a non-linear dashpot. The data demonstrated that a model calibrated using data from experiments performed at low and intermediate strain rates, but was able to predict the response in high strain rate loading up to 1220 s^{-1}. The model was also able to capture strain recovery after compression, and cyclic loading. As well as being applicable to the practical use of this material, the model shows the value of using predictive approaches to measure the high strain rate response, which can be difficult to measure directly. Further research is ongoing to implement this into a model for composites based on this material.

8 CRediT authorship contribution statement

Huanming CHEN: Conceptualization, Methodology, Validation, Formal analysis, Investigation, Software, Writing - original draft. **Lewis R. Hart**: Investigation, Visualization, Software, Formal analysis, Writing - review & edit. **Wayne Hayes**: Resources, Visualization, Formal analysis, Writing - review & edit. **Clive R. Siviour**: Resources, Conceptualization, Project administration, Supervision, Writing - review & edit.

9 Declaration of competing interest

The authors declare that they have no known competing financial interests or personal relationships that could have appeared to influence the work reported in this paper

10 Acknowledgements

This material is based upon work supported by the Air Force Office of Scientific Research, Air

Force Material Command, USAF under Award No. FA9550-15-1-0448. The funders had no involvement in study design, collection, analysis and interpretation of data, writing of the report or the decision to submit the article for publication. We are also grateful to the University of Reading for and access to the analytical instrumentation within the Chemical Analysis Facility, we also thank EPSRC (EP/N024818/1) for post-doctoral research fellowship in support of LRH. We thank Prof. Paul Buckley, at Oxford University, for insight and expertise in polymer research. We also would like to thank Igor Dyson for technical support at Oxford University and, in particular, Nick Hawkins for invaluable support with the experiments on the rheometer and DMA.

11 Supplementary data

Supplementary data to this article can be found online.

12 Data availability

The raw/processed data to support this article can be found online:

http://dx.doi.org/10.17632/tby33jd48k.1

13 References

[1] K. Chino, M. Ashiura, Themoreversible cross-linking rubber using supramolecular hydrogen-bonding networks, Macromolecules. 34 (2001) 9201–9204.

DOI: 10.1021/ma011253v

[2] S. Burattini, B.W. Greenland, D. Chappell, H.M. Colquhoun, W. Hayes, Healable polymeric materials: a tutorial review, Chem. Soc. Rev. 39 (2010) 1973–1985.

DOI: 10.1039/b904502n

[3] L.M. de Espinosa, G.L. Fiore, C. Weder, E.J. Foster, Y.C. Simon, Healable supramolecular polymer solids, Prog. Polym. Sci. 49 (2015) 60–78.

https://doi.org/10.1016/j.progpolymsci.2015.04.003

[4] L.R. Hart, J.L. Harries, B.W. Greenland, H.M. Colquhoun, W. Hayes, Healable supramolecular polymers, Polym. Chem. 4 (2013) 4860–4870.

DOI: 10.1039/C3PY00081H

[5] W.M. Huang, B. Yang, Y. Zhao, Z. Ding, Thermo-moisture responsive polyurethane shape-memory polymer and composites: a review, J. Mater. Chem. 20 (2010) 3367–3381.

DOI: 10.1039/B922943D

[6] G. Rivero, L.-T.T. Nguyen, X.K.D. Hillewaere, F.E. Du Prez, One-pot thermo-remendable shape memory polyurethanes, Macromolecules. 47 (2014) 2010–2018.

DOI: 10.1021/ma402471c

[7] A. Feula, A. Pethybridge, I. Giannakopoulos, X. Tang, A. Chippindale, C.R. Siviour, C.P. Buckley, I.W. Hamley, W. Hayes, A Thermoreversible Supramolecular Polyurethane with Excellent Healing Ability at 45 °C, Macromolecules. 48 (2015) 6132–6141.

https://doi.org/10.1021/acs.macromol.5b01162.

[8] A. Feula, X. Tang, I. Giannakopoulos, A.M. Chippindale, I.W. Hamley, F. Greco, C. Paul Buckley, C.R. Siviour, W. Hayes, An adhesive elastomeric supramolecular polyurethane healable at body temperature, Chem. Sci. 7 (2016) 4291–4300. https://doi.org/10.1039/C5SC04864H.

[9] Z.S. Petrović, J. Ferguson, Polyurethane elastomers, Prog. Polym. Sci. 16 (1991) 695–836.

DOI: 10.1016/0079-6700(91)90011-9

[10] J.T. Koberstein, A.F. Galambos, L.M. Leung, Compression-molded polyurethane block copolymers. 1. Microdomain morphology and thermomechanical properties, Macromolecules. 25 (1992) 6195–6204.

DOI: 10.1021/ma00049a017

[11] R. Stadler, L. de Lucca Freitas, Thermoplastic elastomers by hydrogen bonding 1. Rheological properties of modified polybutadiene, Colloid Polym. Sci. 264 (1986) 773–778.

DOI: 10.1007/BF01500752

[12] R.F.M. Lange, M. Van Gurp, E.W. Meijer, Hydrogen-bonded supramolecular polymer networks, J. Polym. Sci. Part A Polym. Chem. 37 (1999) 3657–3670.

DOI: 10.1002/(SICI)1099-0518(19991001)37:19<3657::AID-POLA1>3.0.CO;2-6

[13] P. Du, M. Wu, X. Liu, Z. Zheng, X. Wang, T. Joncheray, Y. Zhang, Diels--Alder-based crosslinked self-healing polyurethane/urea from polymeric methylene diphenyl diisocyanate, J. Appl. Polym. Sci. 131 (2014).

DOI: 10.1002/app.40234

[14] C.L. Elkins, T. Park, M.G. McKee, T.E. Long, Synthesis and characterization of poly (2-ethylhexyl methacrylate) copolymers containing pendant, self-complementary multiple-hydrogen-bonding sites, J. Polym. Sci. Part A Polym. Chem. 43 (2005) 4618–4631.

DOI: 10.1002/pola.20961

[15] X. Tang, A. Feula, B.C. Baker, K. Melia, D.H. Merino, I.W. Hamley, C.P. Buckley, W. Hayes, C.R. Siviour, A dynamic supramolecular polyurethane network whose mechanical properties are kinetically controlled, Polymer (Guildf). 133 (2017) 143–150.

DOI: 10.1016/j.polymer.2017.11.005

[16] P.J. Woodward, D. Hermida Merino, B.W. Greenland, I.W. Hamley, Z. Light, A.T. Slark, W. Hayes, Hydrogen bonded supramolecular elastomers: correlating hydrogen bonding strength with morphology and rheology, Macromolecules. 43 (2010) 2512–2517.

DOI: 10.1021/ma9027646

[17] J. Courtois, I. Baroudi, N. Nouvel, E. Degrandi, S. Pensec, G. Ducouret, C. Chanéac, L. Bouteiller, C. Creton, Supramolecular soft adhesive materials, Adv. Funct. Mater. 20 (2010) 1803–1811.

DOI: 10.1002/adfm.200901903

[18] S. Salimi, L.R. Hart, A. Feula, D. Hermida-Merino, A.B.R. Touré, E.A. Kabova, L. Ruiz-Cantu, D.J. Irvine, R. Wildman, K. Shankland, others, Property enhancement of healable supramolecular polyurethanes, Eur. Polym. J. 118 (2019) 88–96.

DOI: 10.1016/j.eurpolymj.2019.05.042

[19] D. Hermida-Merino, B. O'Driscoll, L.R. Hart, P.J. Harris, H.M. Colquhoun, A.T. Slark, C. Prisacariu, I.W. Hamley, W. Hayes, Enhancement of microphase ordering and mechanical properties of supramolecular hydrogen-bonded polyurethane networks, Polym. Chem. 9 (2018) 3406–3414.

DOI: 10.1039/C8PY00604K

[20] V. Simic, L. Bouteiller, M. Jalabert, Highly cooperative formation of bis-urea based supramolecular polymers, J. Am. Chem. Soc. 125 (2003) 13148–13154.

DOI: 10.1021/ja037589x

[21] D.H. Merino, A.T. Slark, H.M. Colquhoun, W. Hayes, I.W. Hamley, Thermo-responsive microphase separated supramolecular polyurethanes, Polym. Chem. 1 (2010) 1263–1271.

DOI: 10.1039/C0PY00122H

[22] K.A. Houton, G.M. Burslem, A.J. Wilson, Development of solvent-free synthesis of hydrogen-bonded supramolecular polyurethanes, Chem. Sci. 6 (2015) 2382–2388.

DOI: 10.1039/C4SC03804E

[23] S. Das, D.F. Cox, G.L. Wilkes, D.B. Klinedinst, I. Yilgor, E. Yilgor, F.L. Beyer, Effect of symmetry and H-bond strength of hard segments on the structure-property relationships of segmented, nonchain extended polyurethanes and polyureas, J. Macromol. Sci. Part B Phys. 46 (2007) 853–875.

DOI: 10.1080/00222340701388805

[24] X. Tang, C.R. Siviour, C.P. Buckley, A. Feula, W. Hayes, Effect of temperature and strain rate on the compressive behaviour of supramolecular polyurethane, in: EPJ Web Conf., 2015: p. 1046.

DOI: 10.1051/epjconf/20159401046

[25] W. Knoben, N.A.M. Besseling, M.A. Cohen Stuart, Rheology of a reversible supramolecular polymer studied by comparison of the effects of temperature and chain stoppers, J. Chem. Phys. 126 (2007) 24907.

DOI: 10.1063/1.2409296

[26] A. Gooch, C. Nedolisa, K.A. Houton, C.I. Lindsay, A. Saiani, A.J. Wilson, Tunable self-assembled elastomers using triply hydrogen-bonded arrays, Macromolecules. 45 (2012) 4723–4729.

DOI: 10.1021/ma3001109

[27] C.R. Siviour, P.R. Laity, W.G. Proud, J.E. Field, D. Porter, P.D. Church, P. Gould, W. Huntingdon-Thresher, High strain rate properties of a polymer-bonded sugar: their dependence on applied and internal constraints, Proc. R. Soc. A Math. Phys. Eng. Sci. 464 (2008) 1229–1255.

DOI: 10.1098/rspa.2007.0214

[28] W.W. Chen, Experimental methods for characterizing dynamic response of soft materials, J. Dyn. Behav. Mater. 2 (2016) 2–14.

DOI: 10.1007/s40870-016-0047-5

[29] C.R. Siviour, J.L. Jordan, High strain rate mechanics of polymers: a review, J. Dyn. Behav. Mater. 2 (2016) 15–32.

DOI: 10.1007/s40870-016-0052-8

[30] C.R. Siviour, High strain rate characterization of polymers, AIP Conf. Proc. 1793 (2017).

https://doi.org/10.1063/1.4971585.

[31] G.T. Gray III, W.R. Blumenthal, Split-Hopkinson pressure bar testing of soft materials, ASM Handb. 8 (2000) 488–496.

https://doi.org/10.31399/asm.hb.v08.a0003298

[32] M.J. Kendall, C.R. Siviour, Rate dependence of poly (vinyl chloride), the effects of plasticizer and time--temperature superposition, Proc. R. Soc. A Math. Phys. Eng. Sci. 470 (2014) 20140012.

DOI: 10.1098/rspa.2014.0012

[33] M.J. Kendall, C.R. Siviour, Experimentally simulating adiabatic conditions: Approximating high rate polymer behavior using low rate experiments with temperature profiles, Polym. (United Kingdom). 54 (2013) 5058–5063. https://doi.org/10.1016/j.polymer.2013.06.049.

[34] H. Chen, A.R. Trivedi, C.R. Siviour, Application of Linear Viscoelastic Continuum Damage Theory to the Low and High Strain Rate Response of Thermoplastic Polyurethane, Exp. Mech. (2020) 1–12.

DOI: 10.1007/s11340-020-00608-2

[35] M. Blain, A. Cornille, B. Boutevin, R. Auvergne, D. Benazet, B. Andrioletti, S. Caillol, Hydrogen bonds prevent obtaining high molar mass PHU s, J. Appl. Polym. Sci. 134 (2017) 44958.

DOI: 10.1002/app.44958

[36] D.K. Chattopadhyay, K. Raju, Structural engineering of polyurethane coatings for high performance applications, Prog. Polym. Sci. 32 (2007) 352–418.

DOI: 10.1016/j.progpolymsci.2006.05.003

[37] P. Krol, Synthesis methods, chemical structures and phase structures of linear polyurethanes. Properties and applications of linear polyurethanes in polyurethane elastomers, copolymers and ionomers, Prog. Mater. Sci. 52 (2007) 915–1015.

DOI: 10.1016/j.pmatsci.2006.11.001

[38] M. Menzinger, R. Wolfgang, The meaning and use of the Arrhenius activation energy, Angew. Chemie Int. Ed. English. 8 (1969) 438–444.

DOI: 10.1002/anie.196904381

[39] M. Peleg, M.D. Normand, M.G. Corradini, The Arrhenius equation revisited, Crit. Rev. Food Sci. Nutr. 52 (2012) 830–851.

DOI: 10.1080/10408398.2012.667460

[40] J.D. Ferry, Viscoelastic properties of polymers, John Wiley & Sons, 1980.

DOI: 10.1016/0377-0257(81)80036-5

[41] M.L. Williams, R.F. Landel, J.D. Ferry, The temperature dependence of relaxation mechanisms in amorphous polymers and other glass-forming liquids, J. Am. Chem. Soc. 77 (1955) 3701–3707.

https://doi.org/10.1021/ja01619a008

[42] I.M. Ward, D.W. Hadley, An introduction to the mechanical properties of solid polymers, 1993.

[43] O.U. Colak, Modeling deformation behavior of polymers with viscoplasticity theory based on overstress, Int. J. Plast. 21 (2005) 145–160.

DOI: 10.1016/j.ijplas.2004.04.004

[44] O.U. Colak, N. Dusunceli, Modeling viscoelastic and viscoplastic behavior of high density polyethylene (HDPE), J. Eng. Mater. Technol. 128 (2006) 572–578.

DOI: 10.1115/1.2345449

[45] H.J. Qi, M.C. Boyce, Constitutive model for stretch-induced softening of the stress-stretch behavior of elastomeric materials, J. Mech. Phys. Solids. 52 (2004) 2187–2205. https://doi.org/10.1016/j.jmps.2004.04.008.

[46] W. Zhang, Y. Cai, Theory of visco-elasto-plastic damage mechanics, in: Contin. Damage Mech. Numer. Appl., Springer, 2010: pp. 589–721.

DOI: 10.1007/978-3-642-04708-4_8

[47] A. Khan, H. Zhang, Finite deformation of a polymer: experiments and modeling, Int. J. Plast. 17 (2001) 1167–1188.

DOI: 10.1016/S0749-6419(00)00073-5

[48] A.S. Khan, O. Lopez-Pamies, R. Kazmi, Thermo-mechanical large deformation response and constitutive modeling of viscoelastic polymers over a wide range of strain rates and temperatures, Int. J. Plast. 22 (2006) 581–601.

DOI: 10.1016/j.ijplas.2005.08.001

[49] M. Sobhanie, A.I. Isayev, Y. Fan, Viscoelastic plastic rheological model for particle filled polymer melts, Rheol. Acta. 36 (1997) 66–81.

DOI: 10.1007/BF00366725

[50] P. Saramito, A new constitutive equation for elastoviscoplastic fluid flows, J. Nonnewton. Fluid Mech. 145 (2007) 1–14.

DOI: 10.1016/j.jnnfm.2007.04.004

[51] M.J. Kendall, D.R. Drodge, R.F. Froud, C.R. Siviour, Stress gage system for measuring very soft materials under high rates of deformation, Meas. Sci. Technol. 25 (2014) 75603.

DOI: 10.1088/0957-0233/25/7/075603

[52] D.A. Gorham, Specimen inertia in high strain-rate compression, J. Phys. D. Appl. Phys. 22 (1989) 1888.

DOI: 10.1088/0022-3727/49/4/043001

[53] C.R. Siviour, S.M. Walley, Inertial and frictional effects in dynamic compression testing, in: Kolsk. Bar Mach., Springer, 2018: pp. 205–247.

DOI: 10.1007/978-3-319-71919-1_8

[54] M. Hockly, C.R. Siviour, Specimen Inertia in high strain rate tensile testing, in: EPJ Web Conf., 2015: p. 1050.

DOI: 10.1051/epjconf/20159401050

[55] R. Kapoor, S. Nemat-Nasser, Determination of temperature rise during high strain rate deformation, Mech. Mater. 27 (1998) 1–12.

DOI: 10.1016/S0167-6636(97)00036-7